Follow us @BoneJointRes

Freely available online OPEN ACCESS

BJR

BIOMECHANICS

Effects of condensation and compressive strain on implant primary stability

A LONGITUDINAL, IN VIVO, MULTISCALE STUDY IN MICE

Z. Li,
M. Arioka,
Y. Liu,
M. Aghvami,
S. Tulu,
J. B. Brunski,
J. A. Helms

Division of Plastic and Reconstructive Surgery, Department of Surgery, Stanford School of Medicine, Stanford, California, USA

Aims

Surgeons and most engineers believe that bone compaction improves implant primary stability without causing undue damage to the bone itself. In this study, we developed a murine distal femoral implant model and tested this dogma.

Methods

Each mouse received two femoral implants, one placed into a site prepared by drilling and the other into the contralateral site prepared by drilling followed by stepwise condensation.

Results

Condensation significantly increased peri-implant bone density but it also produced higher strains at the interface between the bone and implant, which led to significantly more bone microdamage. Despite increased peri-implant bone density, condensation did not improve implant primary stability as measured by an in vivo lateral stability test. Ultimately, the condensed bone underwent resorption, which delayed the onset of new bone formation around the implant.

Conclusion

Collectively, these multiscale analyses demonstrate that condensation does not positively contribute to implant stability or to new peri-implant bone formation.

Cite this article: *Bone Joint Res.* 2020;9(2):60–70.

Keywords: Implant, Bone resorption, Biomechanical, Osseointegration

Article focus

- The aim of this study was to combine an engineering outlook with a biological perspective on how different methods of site preparation specifically impact peri-implant strain and bone remodelling around an implant.

Key messages

- Bone preparing by condensation does not enhance stability of an implant better than preparation by drilling in the implant site.
- New bone formation leads to secondary implant stability, so any delay in this biological process can jeopardize long-term implant stability.
- This study lays the groundwork for devising new methods for implant site preparation that simultaneously preserve the trabecular network, which provides implant stability, while avoiding thermal-induced apoptosis and necrosis associated with drilling.

Strengths and limitations

- This study combined the engineering outlook with a biological perspective on different methods of site preparation in the mouse model.
- A murine model would have the added benefit of being amenable to a comprehensive tissue, cell, and molecular analysis of implant site preparation.
- Although there is a difference in size, microstructural characteristics between humans and mice are similar and a murine model has the benefit of being amenable to a comprehensive tissue, cell, and molecular analysis of implant site preparation.

Correspondence should be sent to J. A. Helms;
email: jhelms@stanford.edu

doi: 10.1302/2046-3758.92.BJR-2019-0161

Bone Joint Res 2020;9:60–70.

Introduction

Arthroplasty surgeries aim to reduce pain and restore function by replacing a damaged joint with a metal prosthesis. Approximately 9% of these arthroplasties will fail within ten years, primarily because the prosthesis loosens over time.[1] In the absence of infection, this is referred to as aseptic loosening and it can have multiple aetiologies. For example, bone resorption (osteolysis) can lead to implant loosening.[2] Likewise, 'stress-shielding' by the implant can cause a reduction in peri-implant bone density (osteopaenia), which can increase the likelihood of aseptic loosening.[3–5] Another factor implicated in aseptic loosening is an 'unfavourable biomechanical environment' that interferes with the initial attachment of bone to the implant.[6] The magnitude and distribution of stresses and strains can also have a profound impact on the biological response from peri-implant bone[4] and these responses can range from osteocyte apoptosis and death, to bone resorption followed by active new bone formation. Ultimately, these events culminate in either an osseointegrated implant, or one that becomes encapsulated in fibrous tissue, but what constitutes a 'safe' versus 'dangerous' level of peri-implant stress/strain is not always clear.

Here, our goal was to combine an engineering outlook with a biological perspective on how different methods of site preparation specifically impact peri-implant strain and bone remodelling around an implant. In order to study this process at the molecular and cellular levels, we employed a mouse model, then modified it to align, as much as possible, with site preparation techniques used in arthroplasty surgeries. For example, in arthroplasty surgeries, site preparation typically involves the production of an initial osteotomy that is gradually enlarged.[7,8] Methods for enlarging the osteotomy include drilling and reaming to remove bone stock and thus allow the larger diameter implant to be placed.[9] In this case, heat generated by drilling can cause thermal necrosis in the bone;[10] consequently, irrigation is often employed in an attempt to cool the drill. In another method called broaching, the osteotomy is enlarged but, instead of removing bone stock, a compressive force is employed. In addition to preserving bone stock, this approach is also thought to 'interlock' the implant into the bone.[11–13]

We replicated both methods of site preparation in the mouse model. Although there is a difference in size, microstructural characteristics such as bone volume/total volume (BV/TV) are strikingly similar between humans and mice.[14–16] Heat transfer in bone is dependent upon its mineral density, which is also comparable between humans and rodents.[17,18] Finally, the material properties, and therefore the strength of both cortical and trabecular bone, are similar.[19–21] Thus, we reasoned that a murine model would be suitable for this study, and it would have the added benefit of being amenable to a comprehensive tissue, cell, and molecular analysis of implant site preparation.

Methods

Animal surgeries. This study's protocols followed Animal Research: Reporting of In Vivo Experiments (ARRIVE) and the Institutional Animal Care and Use Committee (IACUC) guidelines (#13146). In total, 47 wild-type BALB/C male (three-month-old) mice were used in this study.

Mice were anaesthetized with an intraperitoneal injection of ketamine/xylazine. A split-body experimental design was employed. An 8 mm incision was made on the skin of the anterior-distal aspect of the right knee, and the knee joint was exposed. Between the condyles, a 0.8 mm osteotomy was produced using a 0.8 mm diameter drill bit (Drill Bit City, Chicago, Illinois, USA) and a hand-held dental engine, running at 100 rpm with saline irrigation. Immediately thereafter, a 0.8 mm diameter, 7 mm length, titanium-6 aluminium-4 vanadium alloy (TiAl6V4) implant was positioned into the bone marrow cavity of the femur. The site was closed with non-resorbable sutures. Osteotomies produced in the right femur served as controls (e.g. the 'drilled' cohort; Figure 1b).

On the left femur, the knee joint was exposed, and between the condyles, a 0.6 mm osteotomy was produced using a 0.6 mm diameter drill bit (Drill Bit City). The 0.6 mm osteotomy was increased in size using four tapered osteotomes of progressively increasing diameter (Supplementary Table i). Each osteotome remained in the osteotomy for one minute before the next largest osteotome was used. The final diameter of the condensed osteotomy was 0.8 mm (Supplementary Table i). Thereafter, a 0.8 mm titanium implant was positioned into the bone marrow cavity of the femur. Osteotomies produced in the left femur therefore served as the test cases in this experiment (e.g. the 'condensed' cohort; Figure 1a).

Buprenorphine as an analgesic was provided to all animals immediately post-surgery and for the following three days. Animals ambulated freely and were housed in a temperature-controlled environment with 12-hour light/dark cycles. Food and water were provided ad libitum. No evidence of infection or prolonged inflammation was detected at any of the surgical sites.

Experimental groups. In keeping with the three Rs (replacement, refinement, and reduction), every effort was made to reduce animal numbers. Table I describes experimental groups, timepoint, and number of samples arranged to correspond with testing modality.

Heat transfer model and finite element analyses. A detailed description of the heat transfer model can be found in the study by Aghvami et al.[10] To calculate temperature distributions during implant site preparation, the heat transfer model used a value of 20% to represent the mean BV/TV of the distal femur and a drill speed of 100 rpm. The heat dissipation and temperature distribution associated with irrigation were calculated to align with the actual surgical methods used.

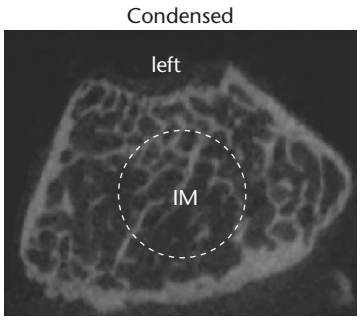

Fig. 1a

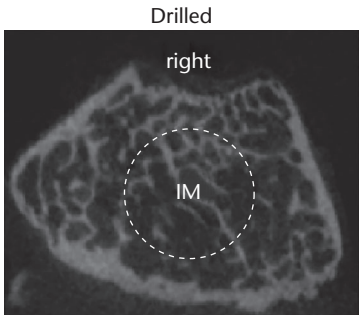

Fig. 1b

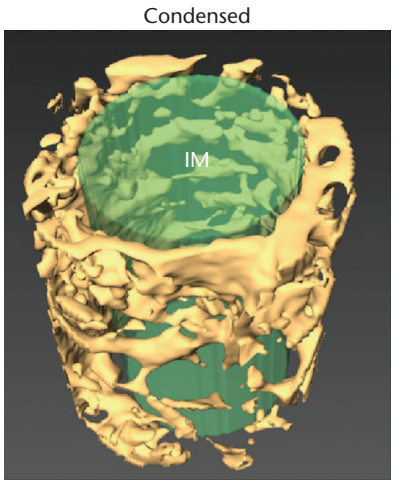

Fig. 1c

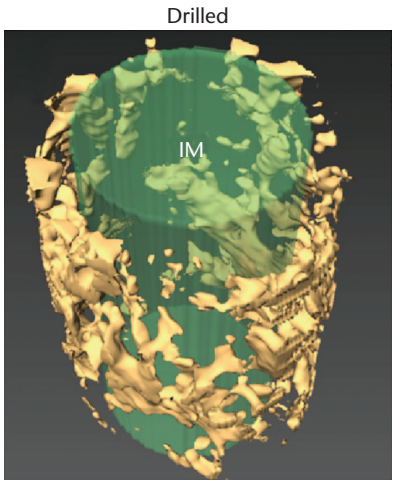

Fig. 1d

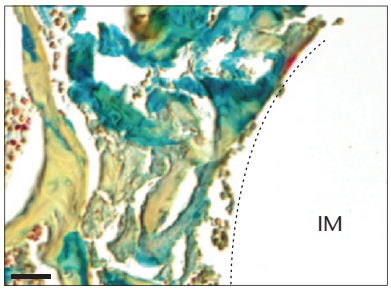

Fig. 1e

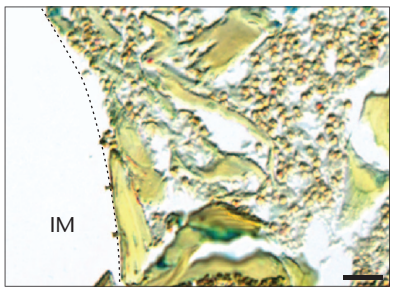

Fig. 1f

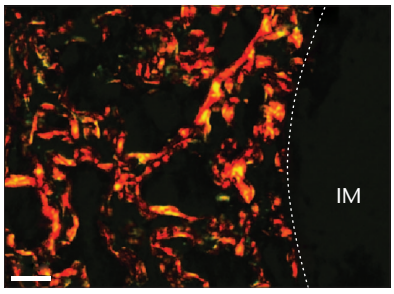

Fig. 1g

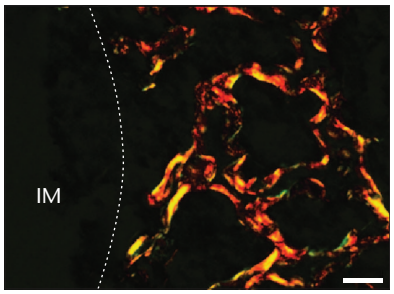

Fig. 1h

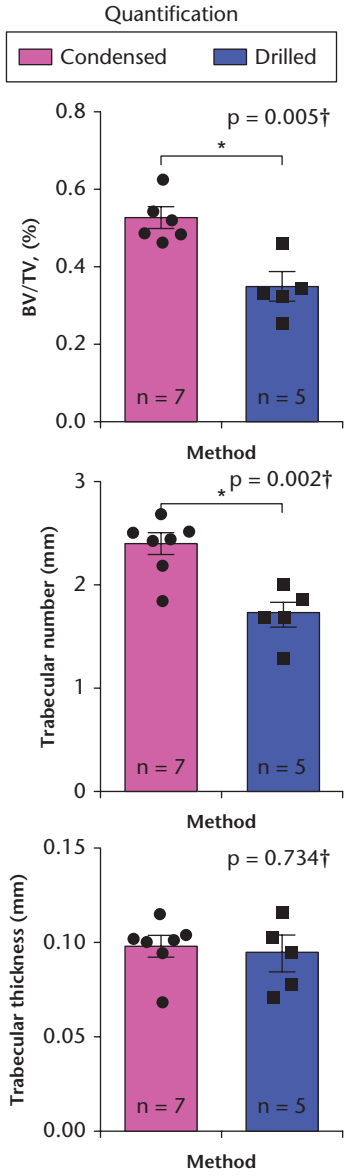

Fig. 1i

Condensation increases bone volume/total volume (BV/TV) of peri-implant bone in the distal femur. In all animals, a) on the left femur, following the pilot drilled, four osteotomies were used in succession. b) On the right femur, osteotomies were accomplished by drilling (grey circle). A titanium alloy implant was then placed in the prepared osteotomies of both sides. c) and d) Volumetric rendering of peri-implant bone (yellow) and the void created by the implant (green) from μCT analyses performed immediately after implant placement. e) and f) Representative pentachrome-stained transverse tissue sections through the distal femur following condensation or drilling, followed by implant placement. Picrosirius Red staining shows bone density increased at g) the interface of bone-implant of the condensation specimens, but not at h) the interface of bone-implant of drilled specimens. i) Quantification of BV/TV, trabecular number, and trabecular thickness from μCT analyses of peri-implant bone following condensation (pink bars) or drilling (blue bars) prior to implant placement. Scale bars = 50 μm. *$p < 0.010$. †Paired *t*-test. IM, implant.

Table I. Distribution of experimental groups across types of analyses

Testing modality	Timepoint (expressed as post-surgery day, PSD)	Condensed bone group (n = number of implants)	Drilled bone group (n = number of implants)
Micro-CT (minus implant)	Day of surgery	7	5
Lateral stability test	Day of surgery	12	12
Histology, TUNEL, TRAP, IHC	Day of surgery	6	6
Histology, TUNEL, TRAP, ALP IHC	3	6	6
Histology, ALP IHC	7	6	6
In vivo bone labelling analysis 1	2.5	5	5
In vivo bone labelling analysis 2	5	5	5

ALP, alkaline phosphatase; IHC, immunohistochemistry; TRAP, tartrate-resistant acid phosphatase; TUNEL, terminal deoxynucleotidyl transferase dUTP nick end labelling.

To estimate the strain distribution in bone due to the condensation procedure, a finite element model (FEM) was formulated in Comsol 5.4 (Stockholm, Sweden). The distal end of the femur was modelled as an axisymmetric cylinder with an outer diameter of 1.5 mm and length 10 mm. Based on the bone's BV/TV of 20%, its Young's elastic modulus was set at 656 MPa, as computed using a power-law relationship between modulus and BV/TV for cancellous bone in rat femora.[22] The bone's Poisson's ratio was set at 0.33. In the proximal region, the femur's inner diameter was initially set at 0.6 mm (to a depth of 10 mm) to simulate the situation after use of the 0.6 mm diameter pilot drill. Each of the subsequent condensation steps (1 to 4) involved stainless steel osteotomes that were tapered over the first 1.6 mm of their length, e.g. the osteotome in step 1 tapered from 0.58 mm to 0.65 mm over a 1.6 mm length, after which the outer diameter remained constant at 0.65 mm. The dimensions of the osteotomes for steps 2, 3, and 4 of the condensation procedures were similar, with tapers of 0.63 mm to 0.7 mm, 0.68 mm to 0.75 mm, and 0.73 mm to 0.8 mm, respectively. The last step in the procedure was the installation of a 0.8 mm diameter implant. To model the insertion of each osteotome and its effects on the bone, the osteotome-bone interface was modelled with a contact pair and coefficient of friction of zero. The tapered end of each osteotome was initially placed 0.35 mm deep into the pilot hole and then displaced 9 mm into the hole left by the previous step. The model was run with geometric non-linearity (Green-Lagrange finite strain), and principal compressive strains were computed in the interfacial bone.

Lateral implant stability test. To assess the stability of the implant in bone, animals were collected immediately after implant placement, tissues were dissected, and were stored in 70% ethanol. A lateral stiffness test was employed where a lateral deflection (Δx) of ~ 30 µm was applied to the implant at 0.5 mm to 0.6 mm above the point where the implant exited the femur. The lateral force (F) required to move the implant 30 µm was recorded. Lateral stiffness, k, was computed using the formula $k = F/\Delta x$. This equation is derived from modelling the implant's lateral tipping movement in bone according to the behaviour of an ideal spring. When measuring the deflection Δx, femora containing the implants were rigidly clamped to a support and positioned in line with a stepper motor (Ultra Motion Digit, Mattituck, New York, USA) equipped with a 10 N load transducer on its moving shaft (Honeywell Model 31; Honeywell, Charlotte, North Carolina, USA). A miniature displacement transducer (MG-DVRT-3; LORD MicroStrain, Williston, Vermont, USA) was positioned on the other side of the implant to directly measure the resulting implant displacement. In the testing protocol, the displacement applied to the implant by the stepper motor was programmed as a triangular displacement versus time waveform, which ramped from zero to a peak displacement of ~ 30 µm in approximately 3.5 seconds; the displacement was then held at the peak value for one second and subsequently returned to zero at the rate at which it was increased (Figure 2). The lateral force on the implant in these tests was ~ 0.1 N to 0.8 N. Given the diameter of the implant and its material (which has an elastic modulus approximately 1,000 times greater than the surrounding bone), the lateral movement (Δx) of the implant was presumed to arise from deformation of the peri-implant bone and not from deformation of the metal.

Image analyses. The distal femur was subjected to µCT analysis at a 10.5 µm resolution (Micro XCT; Xradia, Pleasanton, California, USA). To prepare tissues for scanning, mice were sacrificed and tissues were fixed in 70% ethanol. Tissue samples were reconstructed and segmented using the data visualization software ScanIP (Version 7.0; Simpleware, Exeter, UK). A 600/1000 µm width/height circular volume of interest (VOI) from the peri-implant bone was chosen for bone microarchitecture analysis. Images were opened, and VOIs were cropped using ImageJ (National Institutes of Health, Bethesda, Maryland, USA), then imported into CTan (Skyscan, Billerica, Massachusetts, USA), where the ratios of BV/TV, trabecular number (Tb.N), and trabecular thickness (Tb.Th) were calculated.

Histology. Animals were sacrificed at postsurgery day (PSD) 0.5, 3, and 7. Tissues were fixed in 4% paraformaldehyde overnight at 4°C then washed in phosphate-buffered saline (PBS) for 30 minutes. Samples were decalcified in 10% ethylenediaminetetraacetic acid (EDTA) for approximately one week. After complete demineralization, specimens were placed in 30% sucrose/PBS

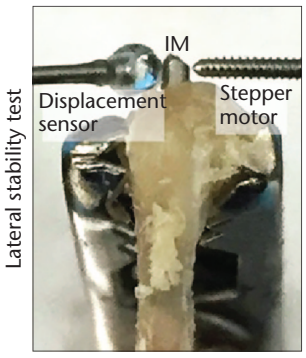

Fig. 2a

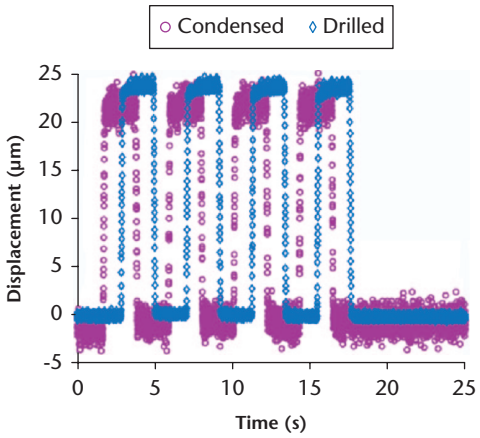

Fig. 2b

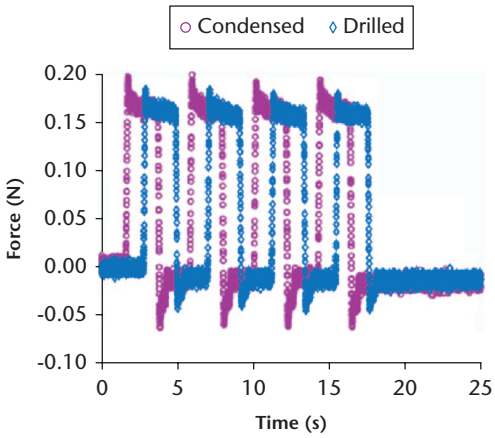

Fig. 2c

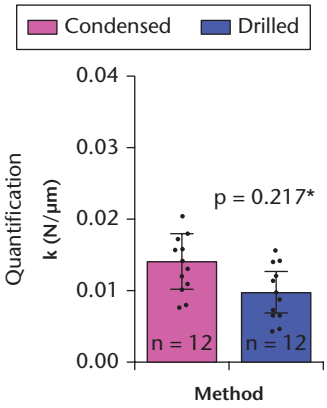

Fig. 2d

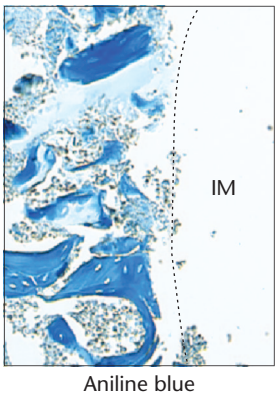

Fig. 2e

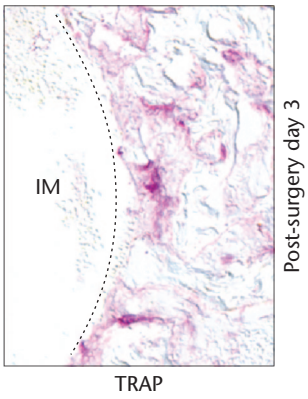

Fig. 2f

Condensation does not improve implant (IM) primary stability. a) Experimental system used to evaluate lateral stability of implants placed in osteotomies created by drilling or condensation. A stepper motor delivered a defined displacement (Δx) at a specified height along the implant, and the resulting force was recorded. b) and c) Representative recordings of force (measured in newtons) and displacement (measured in microns) from a trial run. Initial mechanical (primary) stability was equivalent, regardless of whether the implant was placed into an osteotomy created by condensation or drilling bone. d) The slope of the F/Δx plot was calculated from the linear portion of the trace quantified. e) Aniline Blue staining and f) tartrate-resistant acid phosphatase (TRAP) activity on representative tissue sections from a case where the implant was placed into condensed group on post-surgery day three; dotted line represents bone-implant interface. *Paired *t*-test.

solution overnight at 4°C. At this point, implants were gently removed before the samples were embedded with Tissue-Tek OCT embedding medium (#23-730-571; Thermo Fisher Scientific; Hampton, New Hampshire, USA). Each transverse section of eight microns thick was cut and collected on SuperFrost Plus slides (Thermo Fisher Scientific). Movat's pentachrome and Picrosirius Red staining were performed as described.[23]

TUNEL, TRAP, ALP, and immunohistochemistry. Terminal deoxynucleotidyl transferase dUTP nick end labelling (TUNEL) staining was performed with In Situ Cell Death Detection Kit (Roche, Basel, Switzerland) and mounted with 4′,6-diamidino-2-phenylindole (DAPI) mounting medium (Vector Laboratories, Burlingame, California, USA). Tartrate-resistant acid phosphatase (TRAP) activity was detected using a leucocyte acid phosphatase staining kit (386A; Sigma Aldrich, St Louis, Missouri, USA). Alkaline phosphatase (ALP) activity was shown by incubation in nitro blue tetrazolium chloride (NBT; Roche), 5-bromo-4-chloro-3-indolyl phosphate (BCIP) (Roche), and nontuberculous mycobacteria (NTM) buffer (100 mM sodium chloride (NaCl), 100 mM Tris pH 9.0, 5 mM magnesium chloride ($MgCl_2$)). TRAP staining and ALP staining slides were dehydrated in a series of ethanol and CitriSolv (#89426-268; VWR International, Radnor, Pennsylvania, USA) and then mounted with Permount mounting medium (Thermo Fisher Scientific) .

Immunostaining was performed: tissue sections were permeabilized with 0.5% TritonX-100 (Thermo Fisher Scientific), and after antigen retrieval, slides were blocked with 5% goat serum (Vector S-1000, Vector Laboratories) for one hour at room temperature. Sections were incubated with primary antibodies overnight at 4°C. After washing the slides with PBS, sections were incubated with Cyanine5 conjugated goat anti-rabbit secondary antibody (A10523; Invitrogen, Carlsbad, California, USA) for 30 minutes, then mounted with DAPI mounting medium (Vector Laboratories). The primary antibodies

used were anti-Osterix (ab22552; Abcam, Cambridge, UK), anti-Cathepsin K (ab19027; Abcam), and anti-Ki67 (ab16667; Abcam).

In vivo bone labelling analysis. One day before surgery, mice were injected intraperitoneally with Calcein (10 mg/kg, dissolved in 0.15M NaCl and 2% sodium bicarbonate ($NaHCO_3$)). In a subset of animals (e.g. those in Analysis 1; Figures 3n to 3q), an Alizarin Red injection (12.5 mg/kg, dissolved in saline solution) was performed 1.5 days after the Calcein injection (Timeline; Figure 3m). Two days later, this subset of animals was sacrificed. Tissues were processed for cryo-embedding (described above). Kawamoto's film method[24] was used to collect tissue sections for analyses of vital dye labelling.

Another subset of mice (e.g. those in Analysis 2; Figures 4h to 4j) was injected intraperitoneally with Alizarin Red four days after the first Calcein labelling injection (see Timeline; Figure 4g). Two days later, this subset of mice was sacrificed, and tissues were processed.

Histomorphometric analyses. To quantify, a region of interest (ROI) was selected that focused on the endosteal bone proximal to the growth plate. This ROI was represented across approximately 50 tissue sections, each of which was 8 μm to 10 μm thick. Of those 50 tissue sections, a minimum of five were used for quantification purposes. Tissue sections were photographed using a Leica digital imaging system (Buffalo Grove, Illinois, USA) by a single investigator (ZL), while quantification and analyses were conducted by two blinded individuals (MA and YL). Pentachrome staining was used to detect new peri-implant bone. In the transverse plane, the ROI extended from the edge of the implant circumferentially outward ~ 600 μm. The number of pixels corresponding to pentachrome-stained new bone in the ROI was calculated and expressed as a percentage of the total number of pixels in the ROI.

A similar ROI was used to process quantifications by in vivo bone labelling. The number of Calcein-positive pixels in the ROI was expressed as a percentage of the total number of pixels in the ROI. The same procedure was used to quantify Alizarin Red-positive pixels.

Statistical analyses. An online tool, 'Sample Size Calculator' by ClinCalc, designed for calculating the minimum sample size for adequate study power, was employed.[25] The actual number of samples generated for each experiment was above the minimum (Table II).

All estimations were performed by setting parameters so that α (type I error) = 0.05, β (type II error) = 0.2, enrolment ratio = 1. In addition, a post hoc power analysis tool, 'Post-hoc Power Calculator'[26], ClinCalc, was employed to verify the power of our results. All comparisons are powered > 95%.

Results were presented as means (SD). A paired *t*-test was used to determine significant differences between datasets. A p-value < 0.05 was considered statistically significant and all statistical analyses were performed with Microsoft Excel software (Version 15.16; Microsoft, Redmond, Washington, USA).

Table II. Power analysis to determine sample size

Experiment	Minimum sample size, n	Actual sample size, n
Figures 1a to 1d, 1i	4	7/5
Figures 1e to 1h	4	6
Figures 2a to 2d	10	12
Figures 2e to 2f	4	6
Figures 3d to 3i	4	6
Figures 3j to 3n	3	5
Figures 4a to 4f, 4k to 4s	4	6
Figures 4g to 4j	3	5

Results

Condensation significantly increases peri-implant bone density. We used μCT analyses to demonstrate that condensation significantly increased the BV/TV of peri-implant bone (Figures 1c and 1d; quantified in Figure 1i). Histologically, condensed samples showed densely packed trabeculae (Figure 1e) whereas the drilled samples had more marrow cells and less bone matrix (Figure 1f). Picrosirius Red staining demonstrated a dense, collagen-rich extracellular matrix around condensed samples (Figures 1g and 1h).

Condensation does not enhance primary stability of an implant. Thus far, our quantitative analyses demonstrated that condensation increased the apparent density of peri-implant bone, just as has been reported in humans.[27] We next tested whether this increase in bone density translated into better mechanical stability of the implant. Lateral stability testing provided a means to directly measure how well an implant resists moving in response to a defined lateral load. In this test, the femur was rigidly fixed to a stage and a stepper motor was programmed to advance towards the implant; a displacement transducer was positioned on the opposite side of the implant to directly measure this displacement (Figure 2a). Since the elastic modulus of the bone is significantly lower than the elastic modulus of the implant itself, any lateral movement of the implant can be ascribed solely to the deformation of the peri-implant bone.

In the condensed bone samples, a 30 μm displacement (Figure 2b) required a peak force of ~ 0.2 N (Figure 2c). For drilled bone samples, the same 30 μm displacement (Figure 2b) required a peak force of ~ 0.18 N (Figure 2c). Therefore, the mechanical stability of implants placed into condensed sites was not superior to those placed into drilled sites (Figure 2d). The reason for this lack of improved stability was suggested by histologic and TRAP analyses, conducted on PSD 3: in condensed samples, the fragments of trabecular bone that were compacted around the implant (Figure 2e) were undergoing resorption (Figure 2f).

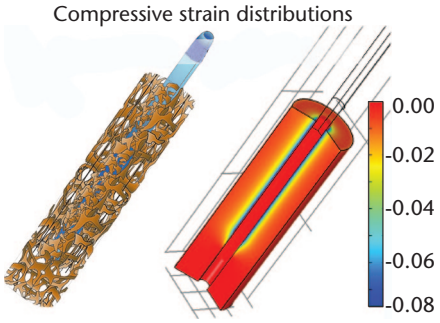

Fig. 3a

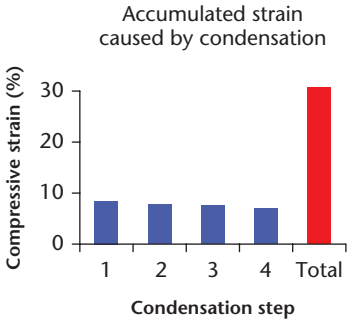

Fig. 3b

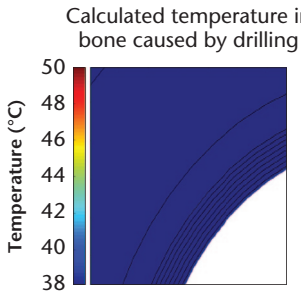

Fig. 3c

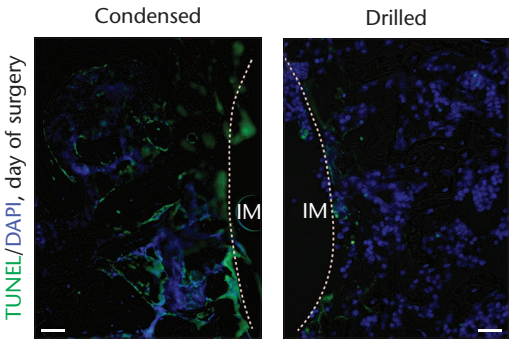

Fig. 3d

Fig. 3e

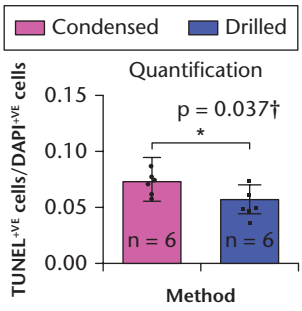

Fig. 3f

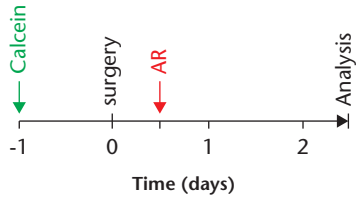

Fig. 3m

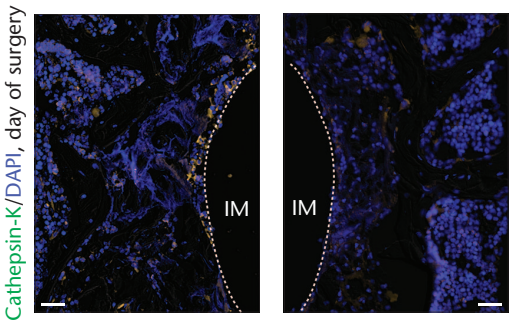

Fig. 3g

Fig. 3h

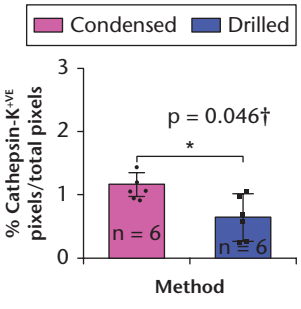

Fig. 3i

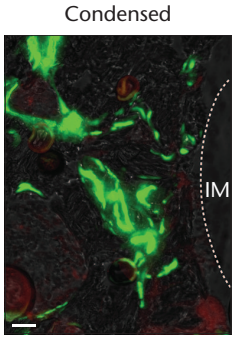

Fig. 3n

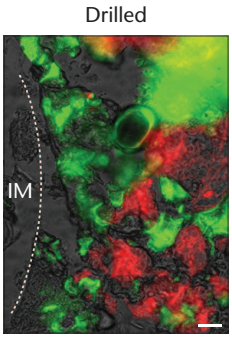

Fig. 3o

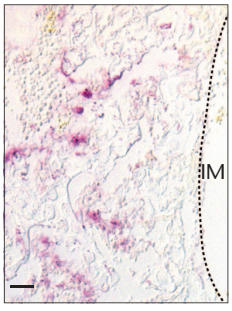

Fig. 3j

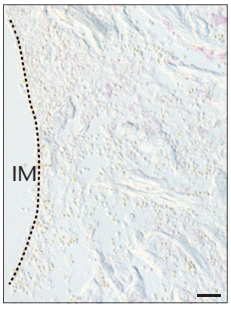

Fig. 3k

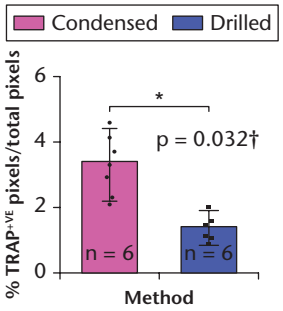

Fig. 3l

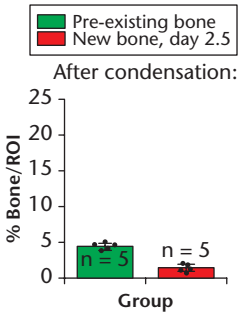

Fig. 3p

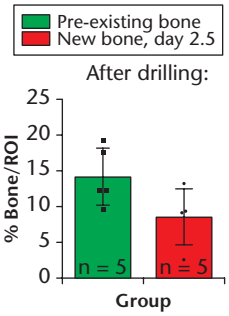

Fig. 3q

Condensation creates high interfacial strain, which triggers osteocyte death and bone resorption. a) A representative image of the pattern and magnitude of the compressive strain distributions followed by its gradual enlargement by condensation. b) Graph showing accumulated strain caused by condensation. c) Computational model of heat transfer by the drilling protocol. d) to f) terminal deoxynucleotidyl transferase dUTP nick end labelling (TUNEL) staining on representative tissue sections from d) a case where the implant was placed into condensed bone versus e) a case where the implant was placed into drilled bone on the day of surgery, quantified in f) dotted line represents bone-implant interface. g) to i) Cathepsin-K expression on representative tissue sections from g) a case where the implant was placed into condensed group and h) a case where the implant was placed into drilled group on the day of surgery, quantified in i) dotted line represents bone-implant interface. j) to l) TRAP activity on representative tissue sections from j) a case where the implant was placed into condensed bone versus k) a case where the implant was placed into drilled bone on the day of surgery, quantified in l) dotted line represents bone-implant interface. m) Schematic demonstrating the experimental strategy of labelling analysis using Calcein and Alizarin Red (AR). n) and o) Calcein (green, labelling the previously existing trabecular bone) and AR (red, labelling the newly formed bone) labelling analysis on representative transverse tissue sections in peri-implant region in a n) condensation specimen and o) drilled specimen. p) and q) Quantification of pre-existing (green) and new peri-implant (red) bone following p) condensation or q) drilling. Scale bars = 50 μm. *p < 0.05. †Paired *t*-test. IM, implant; ROI, region of interest; TRAP, tartrate-resistant acid phosphatase.

Condensation stimulates bone resorption while drilled sites are associated with earlier new bone formation. So far, we have demonstrated that condensation significantly increased peri-implant density, but it simultaneously damaged the trabecular architecture and therefore weakened the bone; as a consequence, implants placed in these sites were no more stable than implants placed into drilled osteotomies. Our next analyses focused on the biomechanical sequelae resulting from condensation versus drilling. From a mechanical perspective, condensation produced compressive strains (Figure 3a). The mean compressive strain for each step was 7.7% (SD 7%), and the sum of compressive strains was approximately 31% (Figure 3b). Drilled cases had no compressive strain because the size of the osteotomy fit the external diameter of the implant. Another mechanical factor we considered was heat caused by drilling. The computed peak temperatures were well below the threshold that triggers osteocyte death (Figure 3c).

Biological responses to these mechanical factors were evaluated. For example, DAPI and TUNEL staining, performed on tissues collected within 12 hours of site preparation, showed minimal peri-implant apoptosis in drilled groups (Figures 3d and 3e; quantified in Figure 3f). Condensation did, however, trigger more bone resorption: two markers of osteoclast activity, Cathepsin K and TRAP activity, were higher in condensation samples compared with drilled samples (Figures 3g, 3h, 3j, and 3k; quantified in Figures 3i and 3l). So, while drilling produced some heat, condensation produced high strains that created significantly more destruction. Our next analyses focused on how the body coped with this damage.

Condensation delays the onset of new peri-implant bone formation. We used vital dye labelling to quantify bone turnover in condensed versus drilled osteotomies. Calcein was delivered the day prior to surgery to label pre-existing bone while Alizarin Red was delivered one half-day after the surgery to monitor bone that formed in response to condensation or drilling. Mice were sacrificed at PSD 2.5 (Figure 3m). In condensation samples, minimal Calcein label was detectable; in contrast, Calcein label was abundant in drilled samples (Figures 3n and 3o; quantified in Figures 3p and 3q). This finding demonstrated that pre-existing bone had undergone more resorption in the condensed group.

To evaluate new bone formation, Alizarin Red staining was quantified. In condensation samples, minimal Alizarin Red label was detectable; in contrast, drilled samples showed significantly more Alizarin Red labelling (Figures 3n and 3o; quantified in Figures 3p and 3q). These data demonstrated that new peri-implant bone formation was more robust in drilled samples.

Condensation is associated with slower peri-implant bone accrual. Initially, the extent of peri-implant apoptosis was equal between the condensed and drilled groups but by PSD 3, apoptosis was considerably greater in the condensation group (Figures 4a to 4c). TRAP activity continued to be higher in the condensed group on PSD 3 (Figures 4d and 4e; quantified in Figure 4f). To validate these immunohistochemical findings, we turned again to vital dye labelling. This time, the second Alizarin Red label was delivered on PSD 3 and evaluated on PSD 5 (Figure 4g). Once again, the drilled group showed faster new bone accrual at PSD 5 (Figures 4h and 4i; quantified in Figure 4j).

By PSD 7, cell proliferation was more robust (Figures 4k and 4l; quantified in Figure 4m), and osteogenic protein expression more widespread (Figures 4n and 4o; quantified in Figure 4p) in the drilled group. Histomorphometric measurements showed significantly more new bone in peri-implant environments of those that had been drilled versus condensed (Figures 4q and 4r; quantified in Figure 4s). Collectively, these analyses demonstrated that early-stage events in the peri-implant environment (e.g. less cell death, less bone resorption, and earlier cell proliferation) resulted in significantly more peri-implant bone formation at later stages of the osseointegration programme.

Discussion

The success of cementless femoral prostheses absolutely depends upon creating a environment around the implant, beginning at the time of insertion. From a biomechanical perspective, this stable mechanical stability facilitates the differentiation of progenitor cells into an osteogenic lineage.[28–31] If the peri-implant environment surrounds an unstable implant, the same progenitor cells differentiate into fibroblasts and the end result is fibrous encapsulation of the implant.[28,32,33] Bone compaction/condensation is often used in an attempt to create a stable mechanical environment.[34] In this procedure, a pilot hole is gradually enlarged through the sequential use of broaches, reamers, osteotomes, or similar surgical tools.[27,35,36] Some in vitro studies indicate that cementless femoral stems placed into condensed bone beds show greater stability than implants placed into drilled bone beds.[12] A theoretical explanation for this effect has been proposed, namely, that the compressed/condensed bone 'springs back' and 'locks' the implant into place.[11,37] Bone does have viscoelastic properties, but this 'springing back' characteristic is only relevant if the deformation induced by condensation/compression is lower than the failure/yield properties of bone.[38,39] In vivo studies align with this viewpoint in that they show only a transient increase in the initial stability of femoral implants placed into condensed versus drilled osteotomies. Our data demonstrated no significant increase in implant stability as a consequence of condensation (Figure 2).

In clinical practice, condensation produces peri-implant strains of approximately 65%.[40] In our mouse model, the peri-implant stains were approximately 31%

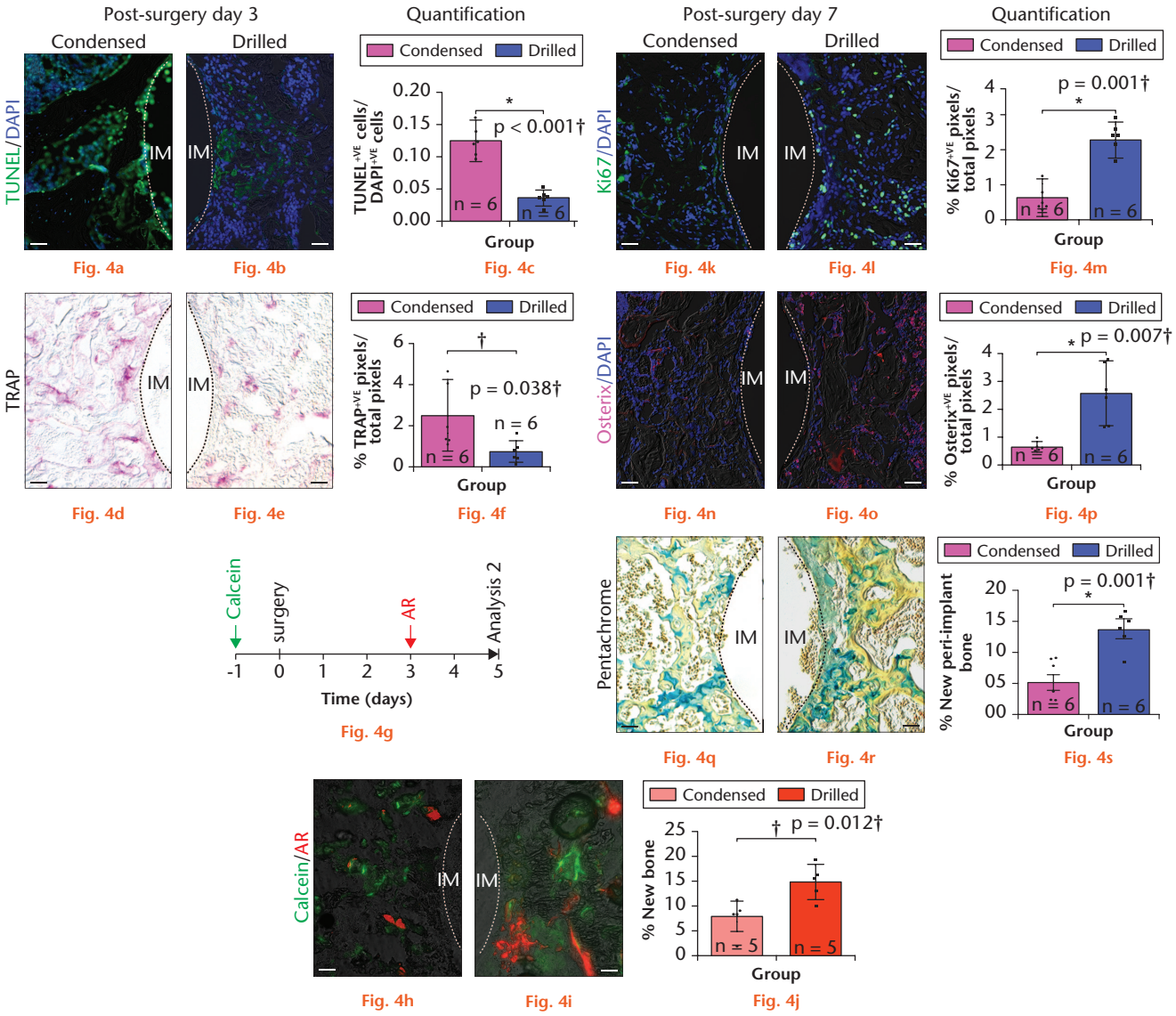

Condensation delays new peri-implant bone formation. a) and b) terminal deoxynucleotidyl transferase dUTP nick end labelling (TUNEL) staining, demonstrating cell apoptosis, on representative transverse tissue sections on post-surgery day (PSD) 3 in a) a case where the implant was placed into condensed bone versus b) a case where the implant was placed into drilled bone. The dotted line represents the bone-implant interface. c) Quantification comparing the ratio of TUNEL-positive with DAPI-positive cells in peri-implant bone following condensation (pink) or drilling (blue). d) to f) TRAP activity on representative tissue sections from d) a case where the implant was placed into condensed bone versus e) a case where the implant was placed into drilled bone on PSD 3, quantified in f). Dotted line represents bone-implant interface. g) Schematic demonstrating the experimental strategy of labelling analysis using Calcein and Alizarin Red (AR). h) and i) Calcein (green, labelling the previously existing trabecular bone) and AR (red, labelling the newly formed bone) labelling analysis on representative transverse tissue sections in peri-implant region from h) a case where the implant was placed into condensed bone versus i) a case where the implant was placed into drilled bone. j) Percentage of new bone in condensation (salmon pink) and drilled (red) groups. k) to m) On PSD 7, the peri-implant region in the k) condensed specimen has fewer Ki67-positive cells compared with that in the l) drilled specimen; quantified in m). n) to p) Similarly, Osterix activity on PSD 7 is lower in the n) condensed specimen compared with in the o) drilled specimen; quantified in p). q) and r) Pentachrome in q) the peri-implant region of a condensed specimen versus r) the peri-implant region of a drilled specimen. s) Quantification of new peri-implant bone in condensed (pink) and drilled (blue) groups. Scale bars = 50 μm. *p < 0.01; †Paired t-test. §p < 0.05. IM, implant; TRAP, tartrate-resistant acid phosphatase.

(Figure 3b). By ensuring that the degree of radial enlargement of the bone bed was on the conservative end of the spectrum in our mouse model, we were able to draw realistic conclusions on how condensation affects peri-implant bone.

Murine implants were purposefully positioned below the surface of the articular cartilage and thus were subjected to nominal loading. This approach was taken for two reasons: first, it removed from consideration the effects of loading-bearing on an implant placed in a quadruped; and second, it represented a conservative approach used by some surgeons for older patients, where bedrest is advised within the first days after implant placement.

Mechanical versus biological stability. In keeping with the clinical claims that condensation/compaction increases peri-implant bone density, we also observed a significant increase in peri-implant BV/TV (Figure 1). Thus, our mouse model aligned with both preclinical[41] and

clinical[42] data showing that compression/condensation increases bone density around an implant.

An assumption is often made that an increase in peri-implant BV/TV should result in an increase in the elastic modulus (e.g. 'stiffness') of the bone, which in turn stabilizes the implant better than a 'softer' bone. This assumption is in alignment with the common power-law relationship between elastic modulus and apparent density.[43] This assumption is unsound. The power-law relationships linking elastic modulus and apparent density were developed from mechanical testing of pristine trabecular bone[43] but this relationship is not applicable to condensed, compacted bone. Using this improper line of reasoning leads to an overestimate of the elastic modulus of condensed bone.

Our data demonstrate that despite a significant increase in peri-implant bone density (Figure 1), there was no accompanying increase in mechanical (primary) stability of the implant (Figure 2). Lateral stability testing data demonstrated that femoral implants placed into condensed osteotomies were no more stable than those placed in drilled osteotomies (Figure 2).

A mechanical perspective on implant site preparation. Drilling generates heat and heat kills osteocytes (Figure 3), so perhaps the damage caused by compression/condensation is offset by the thermal necrosis related to drilling? We tested this possibility but when we examined the extent of programmed cell death and bone resorption, both were higher in the condensed group compared with the drilled group (Figure 3). Vital dye labelling confirmed the molecular/cellular analyses: compared with drilling, condensed sites had significantly less pre-existing bone (e.g. bone resorption predominated; Figure 3) and significantly less new bone (e.g. bone formation was delayed; Figure 4).

Condensation/compaction does not produce thermal necrosis, but it does produce very high peri-implant compressive strains (Figure 3). The act of compression/condensation damaged the connectivity between the bony trabeculae and since trabecular bone derives its strength from its connectivity,[44–47] the end result was that the peri-implant bone was weakened and therefore less able to stabilize the implant compared with the drilled bone.

Improving implant site preparation. Some clinicians believe that the condensation/compaction technique is required for cementless or revision arthroplasties, although there is a recognition that the long-term consequences of condensation/compaction with regard to remodelling are still unclear.[48] Our data underscore the relationship between condensation, the resulting damage, and peri-implant bone resorption (Figures 3 and 4). Vital dye labelling demonstrated that the prolonged bone resorption seen in condensed samples affected the rate of subsequent new bone formation (Figure 4). We speculate as to why this resorptive process precludes new bone formation. In the early stages of bone healing, macrophages remove the provisional fibrin matrix and necrotic cells via phagocytosis, while monocyte-derived osteoclasts resorb the necrotic bone. In addition to removing the cell and extracellular debris, macrophages secrete a range of inflammatory mediators.[49–51] We speculate that in the event of condensation-induced damage, this inflammatory response persists and therefore delays the onset of new bone formation. It is the advent of new bone formation that leads to secondary implant stability and any delay in this biological process may jeopardize long-term implant stability.

In conclusion, in an attempt to improve implant stability, it may initially appear reasonable to increase peri-implant bone density via condensation. While cadaveric studies support this hypothesis, the biological sequelae of condensation argue against it. In a rodent model, condensation did increase peri-implant bone density, but this did not result in improved primary stability because compacted bone was weaker than an intact trabecular network. This study lays the groundwork for devising new methods for implant site preparation that simultaneously preserve the trabecular network-which provides implant stability-while avoiding thermal-induced apoptosis and necrosis associated with drilling.

Supplementary Material

Summary of distal femur preparation and implant placement.

References

1. **Cavalli L, Brandi ML.** Periprosthetic bone loss: diagnostic and therapeutic approaches. *F1000Res.* 2014;2:266.
2. **Moran MM, Wilson BM, Ross RD, Virdi AS, Sumner DR.** Arthrotomy-based preclinical models of particle-induced osteolysis: A systematic review. *J Orthop Res.* 2017;35(12):2595-2605.
3. **Yamako G, Janssen D, Hanada S, et al.** Improving stress shielding following total hip arthroplasty by using a femoral stem made of β type Ti-33.6Nb-4Sn with a Young's modulus gradation. *J Biomech.* 2017;63:135-143.
4. **Sumner DR.** Long-term implant fixation and stress-shielding in total hip replacement. *J Biomech.* 2015;48(5):797-800.
5. **Huiskes R, Weinans H, van Rietbergen B.** The relationship between stress shielding and bone resorption around total hip stems and the effects of flexible materials. *Clin Orthop Relat Res.* 1992;(274):124-134.
6. **Folgado J, Fernandes PR, Jacobs CR, Pellegrini VD Jr.** Influence of femoral stem geometry, material and extent of porous coating on bone ingrowth and atrophy in cementless total hip arthroplasty: an iterative finite element model. *Comput Methods Biomech Biomed Engin.* 2009;12(2):135-145.
7. **Romagnoli S.** Press-fit hip arthroplasty: a European alternative. *J Arthroplasty.* 2002;17(4 Suppl 1):108-112.
8. **Walker PS, Schneeweis D, Murphy S, Nelson P.** Strains and micromotions of press-fit femoral stem prostheses. *J Biomech.* 1987;20(7):693-702.
9. **Otani T, Whiteside LA, White SE, McCarthy DS.** Reaming technique of the femoral diaphysis in cementless total hip arthroplasty. *Clin Orthop Relat Res.* 1995;(311):210-221.
10. **Aghvami M, Brunski JB, Serdar Tulu U, Chen CH, Helms JA.** A Thermal and Biological Analysis of Bone Drilling. *J Biomech Eng.* 2018;140(10).
11. **Kold S, Rahbek O, Vestermark M, Overgaard S, Søballe K.** Bone compaction enhances fixation of weight-bearing hydroxyapatite-coated implants. *J Arthroplasty.* 2006;21(2):263-270.
12. **Chareancholvanich K, Bourgeault CA, Schmidt AH, Gustilo RB, Lew WD.** In vitro stability of cemented and cementless femoral stems with compaction. *Clin Orthop Relat Res.* 2002;(394):290-302.
13. **Green JR, Nemzek JA, Arnoczky SP, Johnson LL, Balas MS.** The effect of bone compaction on early fixation of porous-coated implants. *J Arthroplasty.* 1999;14(1):91-97.

14. **Sell CA, Masi JN, Burghardt A, Newitt D, Link TM, Majumdar S.** Quantification of trabecular bone structure using magnetic resonance imaging at 3 Tesla—calibration studies using microcomputed tomography as a standard of reference. *Calcif Tissue Int.* 2005;76(5):355-364.
15. **Chen CH, Wang L, Serdar Tulu U, et al.** An osteopenic/osteoporotic phenotype delays alveolar bone repair. *Bone.* 2018;112:212-219.
16. **Arioka M, Zhang X, Li Z, et al.** Osteoporotic changes in the periodontium impair alveolar bone healing. *J Dent Res.* 2019;98(4):450-458.
17. **Willinghamm MD, Brodt MD, Lee KL, Stephens AL, Ye J, Silva MJ.** Age-related changes in bone structure and strength in female and male BALB/c mice. *Calcif Tissue Int.* 2010;86(6):470-483.
18. **Ferguson VL, Ayers RA, Bateman TA, Simske SJ.** Bone development and age-related bone loss in male C57BL/6J mice. *Bone.* 2003;33(3):387-398.
19. **Vashishth D.** Small animal bone biomechanics. *Bone.* 2008;43(5):794-797.
20. **Hayes WC, Bouxsein ML.** Biomechanics of cortical and trabecular bone: Implications for assessment of fracture risk. In: Mow VC, Hayes WC, eds. *Basic Orthopaedic Biomechanics.* Philadelphia, Pennsylvania: Lippincott-Raven. 1997:69-111.
21. **Schriefer JL, Robling AG, Warden SJ, Fournier AJ, Mason JJ, Turner CH.** A comparison of mechanical properties derived from multiple skeletal sites in mice. *J Biomech.* 2005;38(3):467-475.
22. **Cory E, Nazarian A, Entezari V, Vartanians V, Müller R, Snyder BD.** Compressive axial mechanical properties of rat bone as functions of bone volume fraction, apparent density and micro-ct based mineral density. *J Biomech.* 2010;43(5):953-960.
23. **Leucht P, Kim JB, Wazen R, et al.** Effect of mechanical stimuli on skeletal regeneration around implants. *Bone.* 2007;40(4):919-930.
24. **Kawamoto T, Kawamoto K.** Preparation of thin frozen sections from nonfixed and undecalcified hard tissues using Kawamot's film method (2012). *Methods Mol Biol.* 2014;1130:149-164.
25. **Dupont WD, Plummer WD Jr.** Power and sample size calculations for studies involving linear regression. *Control Clin Trials.* 1998;19(6):589-601.
26. **Levine M, Ensom MH.** Post hoc power analysis: an idea whose time has passed? *Pharmacotherapy.* 2001;21(4):405-409.
27. **Hjorth MH, Stilling M, Søballe K, Nielsen PT, Christensen PH, Kold S.** Preparation of the femoral bone cavity in cementless stems: broaching versus compaction. *Acta Orthop.* 2016;87(6):575-582.
28. **Cha JY, Pereira MD, Smith AA, et al.** Multiscale analyses of the bone-implant interface. *J Dent Res.* 2015;94(3):482-490.
29. **Yuan X, Pei X, Zhao Y, Tulu US, Liu B, Helms JA.** A Wnt-Responsive PDL Population Effectuates Extraction Socket Healing. *J Dent Res.* 2018;97(7):803-809.
30. **Li J, Yin X, Huang L, et al.** Relationships among Bone Quality, Implant Osseointegration, and Wnt Signaling. *J Dent Res.* 2017;96(7):822-831.
31. **Leucht P, Kim JB, Currey JA, Brunski J, Helms JA.** FAK-Mediated mechanotransduction in skeletal regeneration. *PLoS One.* 2007;2(4):e390.
32. **Yin X, Li J, Chen T, et al.** Rescuing failed oral implants via Wnt activation. *J Clin Periodontol.* 2016;43(2):180-192.
33. **Wazen RM, Currey JA, Guo H, Brunski JB, Helms JA, Nanci A.** Micromotion-induced strain fields influence early stages of repair at bone-implant interfaces. *Acta Biomater.* 2013;9(5):6663-6674.
34. **Bishop NE, Burton A, Maheson M, Morlock MM.** Biomechanics of short hip endoprostheses—the risk of bone failure increases with decreasing implant size. *Clin Biomech (Bristol, Avon).* 2010;25(7):666-674.
35. **Young PS, Patil S, Meek RMD.** Intraoperative femoral fractures: prevention is better than cure. *Bone Joint Res.* 2018;7(1):103-104.
36. **Greenhill DA, Abbasi P, Darvish K, Star AM.** Broach Handle Design Changes Force Distribution in the Femur During Total Hip Arthroplasty. *J Arthroplasty.* 2017;32(6):2017-2022.
37. **Kold S, Bechtold JE, Ding M, Chareancholvanich K, Rahbek O, Søballe K.** Compacted cancellous bone has a spring-back effect. *Acta Orthop Scand.* 2003;74(5):591-595.
38. **Oftadeh R, Perez-Viloria M, Villa-Camacho JC, Vaziri A, Nazarian A.** Biomechanics and mechanobiology of trabecular bone: a review. *J Biomech Eng.* 2015;137(1).
39. **Kopperdahl DL, Keaveny TM.** Yield strain behavior of trabecular bone. *J Biomech.* 1998;31(7):601-608.
40. **Moutsatsos IK, Turgeman G, Zhou S, et al.** Exogenously regulated stem cell-mediated gene therapy for bone regeneration. *Mol Ther.* 2001;3(4):449-461.
41. **Kold S, Rahbek O, Toft M, Ding M, Overgaard S, Søballe K.** Bone compaction enhances implant fixation in a canine gap model. *J Orthop Res.* 2005;23(4):824-830.
42. **Kuzyk PR, Schemitsch EH.** The basic science of peri-implant bone healing. *Indian J Orthop.* 2011;45(2):108-115.
43. **O'Mahony AM, Williams JL, Katz JO, Spencer P.** Anisotropic elastic properties of cancellous bone from a human edentulous mandible. *Clin Oral Implants Res.* 2000;11(5):415-421.
44. **Keaveny TM, Wachtel EF, Guo XE, Hayes WC.** Mechanical behavior of damaged trabecular bone. *J Biomech.* 1994;27(11):1309-1318.
45. **Kabel J, Odgaard A, van Rietbergen B, Huiskes R.** Connectivity and the elastic properties of cancellous bone. *Bone.* 1999;24(2):115-120.
46. **Szabó ME, Zekonyte J, Katsamenis OL, Taylor M, Thurner PJ.** Similar damage initiation but different failure behavior in trabecular and cortical bone tissue. *J Mech Behav Biomed Mater.* 2011;4(8):1787-1796.
47. **Hardisty MR, Zauel R, Stover SM, Fyhrie DP.** The importance of intrinsic damage properties to bone fragility: a finite element study. *J Biomech Eng.* 2013;135(1):011004.
48. **Channer MA, Glisson RR, Seaber AV, Vail TP.** Use of bone compaction in total knee arthroplasty. *J Arthroplasty.* 1996;11(6):743-749.
49. **Wu AC, Raggatt LJ, Alexander KA, Pettit AR.** Unraveling macrophage contributions to bone repair. *Bonekey Rep.* 2013;2:373.
50. **Bielby R, Jones E, McGonagle D.** The role of mesenchymal stem cells in maintenance and repair of bone. *Injury.* 2007;38 Suppl 1:S26-S32.
51. **Kon T, Cho TJ, Aizawa T, et al.** Expression of osteoprotegerin, receptor activator of NF-kappaB ligand (osteoprotegerin ligand) and related proinflammatory cytokines during fracture healing. *J Bone Miner Res.* 2001;16(6):1004-1014.

Author information

- Z. Li, MD, PhD, Postdoctoral researcher, Division of Plastic and Reconstructive Surgery, Department of Surgery, Stanford School of Medicine, Stanford, California, USA; Orthopedic surgeon, Department of Orthopedics, Tianjin Medical University General Hospital, Tianjin, China.
- M. Arioka, DDS, PhD, Visiting scholar, Division of Plastic and Reconstructive Surgery, Department of Surgery, Stanford School of Medicine, Stanford, California, USA; Assistant professor, Department of Clinical Pharmacology, Faculty of Medical Sciences, Kyushu University, Fukuoka, Japan.
- Y. Liu, DDS, PhD, Visiting scholar, Division of Plastic and Reconstructive Surgery, Department of Surgery, Stanford School of Medicine, Stanford, California, USA; Oral surgeon, State Key Laboratory of Oral Diseases, National Clinical Research Center for Oral Diseases, West China Hospital of Stomatology, Sichuan University, Chengdu, China.
- M. Aghvami, PhD, Postdoctoral researcher, Division of Plastic and Reconstructive Surgery, Department of Surgery, Stanford School of Medicine, Stanford, California, USA.
- S. Tulu, PhD, Manager, Division of Plastic and Reconstructive Surgery, Department of Surgery, Stanford School of Medicine, Stanford, California, USA.
- J. B. Brunski, PhD, Professor, Division of Plastic and Reconstructive Surgery, Department of Surgery, Stanford School of Medicine, Stanford, California, USA.
- J. A. Helms, DDS, PhD, Professor, Division of Plastic and Reconstructive Surgery, Department of Surgery, Stanford School of Medicine, Stanford, California, USA.

Author Contributions

- Z. Li: Conceptualized and designed the study, Acquired, analyzed, and interpreted the data, Drafted the manuscript.
- M. Arioka: Acquired, analyzed, and interpreted the data, Drafted the manuscript.
- Y. Liu: Acquired, analyzed, and interpreted the data, Drafted the manuscript.
- M. Aghvami: Acquired, analyzed, and interpreted the data, Drafted the manuscript.
- S. Tulu: Acquired, analyzed, and interpreted the data, Drafted the manuscript.
- J. B. Brunski: Acquired, analyzed, and interpreted the data, Drafted the manuscript.
- J. A. Helms: Conceptualized and designed the study, Analyzed and interpreted the data, Drafted the manuscript.

Funding statement

- One of the authors has received benefits for personal or professional use from a commercial party related indirectly to the subject of this article.

ICMJE COI statement

- J. Brunski reports payments from Nobel Biocare for consultancy and lectures.

Acknowledgements

- This research project was supported by a grant from the National Institutes of Health (R01DE024000-11, JAH and JB). We thank Bo Liu and Xue Yuan for critical insight into the manuscript, and Xiaohui Zhang and Qiang Sun for invaluable aid in performing histology and data analyses.

Ethical review statement

- This study's protocols followed Animal Research: Reporting of In Vivo Experiments (ARRIVE) and the Institutional Animal Care and Use Committee (IACUC) guidelines (#13146). This study did not require ethical approval.